Article:
Walsh, J., Li, D., Chen, Y. et al. (2026) Laminar flame speeds of dimethyl ether-propane/butane/propylene air mixtures. Frontiers in Fuels, 4. 1825931. ISSN: 2813-6217

https://doi.org/10.3389/ffuel.2026.1825931

frontiers in Fuels

TYPE Original Research
PUBLISHED 23 June 2026
DOI 10.3389/ffuel.2026.1825931

OPEN ACCESS

EDITED BY
Ram Ratnakar,
Shell, United States

REVIEWED BY
Ziyu Liu,
Beihang University, China
Thomas Lauer,
Vienna University of Technology, Austria

*CORRESPONDENCE
Ruoyang Yuan,
ruoyang.yuan@sheffield.ac.uk

†PRESENT ADDRESS
Yangming Chen,
Harbin Cigarette Factory of Heilongjiang Tobacco Industry Co., Ltd. Harbin, China

RECEIVED 08 March 2026
REVISED 11 May 2026
ACCEPTED 18 May 2026
PUBLISHED 23 June 2026

CITATION
Walsh J, Li D, Chen Y, Zhang Y and Yuan R (2026) Laminar flame speeds of dimethyl ether-propane/butane/propylene air mixtures.
Front. Fuels 4:1825931.
doi: 10.3389/ffuel.2026.1825931

Laminar flame speeds of dimethyl ether-propane/butane/propylene air mixtures

Jordan Walsh[1], Dezheng Li[2], Yanming Chen[3†], Yang Zhang[2] and Ruoyang Yuan[1*]

[1]School of Mechanical, Aerospace and Civil Engineering, University of Sheffield, Sheffield, United Kingdom, [2]Thermal Engineering Department, Tsinghua University, Beijing, China, [3]Shandong University of Science and Technology, Qingdao, Shandong, China

Introduction: Dimethyl ether (DME) has potential to be used both blended with or as an alternative to Liquefied Petroleum Gas (LPG) to reduce the carbon emissions of a fuel used globally for cooking and heating. Standards to enable the adoption of this require flame speed measurements of the blends of these fuels.
Methods: Measurements of counterflow premixed flame speeds for blends of DME, propane, butane, and propylene at fuel-air equivalence ratios (φ) from 0.75 to 1.6 have been made. These measurements were taken to fill a gap in the current published datasets that primarily have focussed on pure fuels and blends of LPGs constituent gases. These measurements have been produced through a mixture of empirical and simulation work.
Results: We found the flame speeds of the blends overall increase from 0.25 m/s at φ = 0.75 to between 0.4 m/s and 0.45 m/s at φ = 1.0 peaking around φ = 1.0 to 1.1 before decreasing as φ increases further.
Discussion: These data will be useful to support the production of industrial standards that allow for greater adoption of renewable DME as an alternative low carbon fuel to fossil LPG.

KEYWORDS
chemical kinetic simulation, counterflow premixed flame, dimethyl ether, laminar flame speed, PIV

1 Introduction

Dimethyl ether (DME) is a low carbon fuel with potential as a replacement for Liquefied Petroleum Gas (LPG). With similar handling and combustion properties it forms an ideal replacement for a fossil fuel used globally, and with a range of production methods DME can be produced locally shortening supply chains and increasing fuel resilience. One potential route for greater DME adoption without the emissions associated with appliance replacement would be to blend DME into LPG at levels where existing equipment can continue to be used also thereby lowering the cost of adoption and allowing for much sooner mitigation of emissions. In order to do this safely greater understanding of the properties of the blended fuels is needed.

In the United Kingdom LPG fits within gas family III for LPG appliances. Whilst gas families are designated using their Wobbe index flame speed is a key part of standards processes used to define the safe limits of appliances. For gas family III propylene is used as a limit gas to test the upper limits of an appliance with regards to flashback. This is due to its higher flame speed than both propane and butane. A comparison of empirical flame speed studies for the individual fuels have shown DME to have a flame speed lower than that of propylene at rich conditions and higher than that of propylene at lean conditions. If a new

fuel blend were to be allowed to be used with existing appliances it would need to be proven that this new fuel blend fits within the same safety envelope as the previous fuel. Flame speed is therefore a key property in proving this.

Whilst flame speed data is available in previous literature for pure and some blends of DME, propane, butane, and propylene there is minimal data (Safdari et al., 2025) applicable to the blends of fuels that would be found in potential real-world conditions should a DME/LPG blend be commercially produced for the United Kingdom market. The lack of data for these potential fuels is what this paper aims to investigate. There is also variation in the data available of the flame speed measurements for the pure fuels and so this paper also aims to measure this for DME.

The literature available on previous flame speed experiments that used LPG and DME use a range of methodologies, however, the two most common methods are the spherical flame method (Lewis and Von Elbe, 1934; Daly et al., 2001; Qin and Ju, 2005; de Vries et al., 2011; Song et al., 2013; Wu et al., 2014; Yu et al., 2014; Chen, 2015; Movaghar et al., 2020; Safdari et al., 2025) and the counterflow stagnation method (Cheng et al., 2006; Wang et al., 2009; Egolfopoulos et al., 2014; Yang et al., 2021). These methodologies are known to have different drawbacks and main sources of error however for both methods there are challenges with extrapolating the stretch rate to zero and errors associated with the methods of doing so, these are compared well by Jayachandran et al. (2015). Konnov et al. (2018) describe the largest issue with the counterflow method to be stretch on the flame due to the external conditions of the burner, these can be mitigated against through careful nozzle design and nozzle spacing. Xiouris et al. (2016) established that for the spherical flame method radiative losses are a key source of error that has been overlooked in the past.

This paper aims to use improvements in the simulation independence and overall accuracy of the counterflow method in recent years through the use of non-linear extrapolation (Egolfopoulos et al., 2014) to provide flame speed data for DME and LPG blends to fill a gap in the publicly available information for fuels that are seeing growing usage. This would help provide clarity on safe blending limits and promote the adoption of renewable gaseous fuels. This would also provide empirical data that could be used to improve simulation mechanisms predictions of the behaviour of blended fuels.

2 Methodology

2.1 Experimental methodology

The experimental set up was comprised of two opposing nozzles arranged to form a counterflow configuration. The top nozzle was fed with nitrogen; the bottom nozzle was fed from the mixing apparatus that produced the fuel blends tested and the range of equivalence ratios for the fuel blends along with the atomised dimethyl silicone oil particles. The fuel blends were defined as seen in Table 1 below and the purity of the constituent gases can be found in Table 2. Both nozzles had annular shrouds to reduce the turbulence and external air effects. These annular shrouds were fed with nitrogen at the lowest speed possible whilst allowing for the counterflow flame sheet to remain stable, an example of which can be seen in Figure 1a. The gases were fed from high pressure cylinders through one-way valves and flashback arrestors into the blending apparatus. The blending apparatus was formed of a number of ALICAT flow controllers (±0.6% of reading, ±0.1% of full scale) arranged to first blend the fuels together and then introduce the majority of the air and then finally the seeding particles and the carrier air for them. Alongside this blending apparatus there are a number of manually controlled needle valves, these were included to adjust the global flame strain without introducing uncertainty in the fuel blend and stoichiometric conditions. For a given fuel blend and equivalence ratio, the fuel and oxidizer flow rates were first set to achieve the target equivalence ratio. The inlet velocity was then varied by tuning the flow control valves to change the total volumetric flow rate. Throughout this procedure, the fuel to oxidizer ratio was kept constant so that the equivalence ratio remained unchanged. As a result, a series of operating points at the same equivalence ratio but different stretch rates could be obtained with a minimum of four distinct stretch rates however the adjustment procedure was continued until flame instability occurred. This valve-based velocity sweep constitutes the standard protocol used for all experimental cases in this study, and it provides the experimental $S_{u,ref}$ and K_{loc} datasets required for subsequent comparison with simulations and for the determination of S_u^0. The seeding particles were illuminated using a 30W continuous wave green laser and imaged at 7002fps using a 4 MP black and white camera focussed on a 30 mm frame centred on the nozzles. These images were processed using PIVlab (Thielicke, 2014; Thielicke and Stamhuis, 2014; Thielicke and Sonntag, 2021; Thielicke, 2022) and then processed and graphed using a nonlinear extrapolation methodology, the early development of which was documented by Davis and Law (1998), but more recently expanded upon using simulation to produce the extrapolation curves by Wang et al. (2009) and with the error calculation method detailed in Zhang et al. (2014).

The images were taken in sets of twenty for each operating condition and processed with the PIVlab MATLAB package using time resolved pairing yielding 19 paired velocity fields per set. An example velocity field can be seen overlaid on the image it was generated from in Figure 1b. The velocity arrays produced by PIVlab were subsequently post-processed to extract the axial velocity along the vertical centreline of the flow field. This centreline velocity was then plotted against the distance from the lower nozzle to produce a stagnation curve $v(y)$, as illustrated in Figure 2 for Fuel 1 at φ = 1.5 under a fixed inlet flow rate (fixed stretch condition). The stagnation curves are the same as those shown in the later section analysing the simulation data however of course contain more experimental noise. This noise was reduced through temporally averaging groups of frames. Whilst this reduces the number of data points in total and therefore could increase the error margins the temporal averaging increases the clarity of the curves and was therefore necessary. The remaining independent realisations (19 per condition) were retained for repeatability assessments and were used to construct the uncertainty reported in subsequent figures. These uncertainties were calculated following the methodology previously used by Zhang (2017) as this considers the number of data points as a part of the uncertainty propagation into the final values.

TABLE 1 Fuel blend names used in this paper and their make-up.

Blend name	Make-up by % mass	Make-up by % volume
Fuel 1	90% propane, 10% dimethyl ether	90.39% propane 9.61% dimethyl ether
Fuel 2	80% propane, 20% dimethyl ether	80.69% propane 19.31% dimethyl ether
Fuel 3	70% propane, 20% dimethyl ether 10% propylene	70.26% propane, 19.22% dimethyl ether, 10.52% propylene
Fuel 4	70% propane, 20% dimethyl ether, 10% butane	72.36% propane, 19.79% dimethyl ether, 7.84% butane
Fuel 5	60% propane, 20% dimethyl ether, 20% butane	63.61% propane, 20.30% dimethyl ether, 16.09% butane
DME	100% dimethyl ether	100% dimethyl ether

TABLE 2 Purity of gases used.

Blend name	Purity (V/V)
N_2	99.9999%
DME	99.5%
Propane	99.9%
Propylene	99.9%
Butane	99.9%
Air	20.66%O_2 79.34%N_2

As shown in Figure 2, the reference flame speed $S_{u,ref}$ is identified at the minimum of the centreline velocity immediately upstream of the flame front. The local stretch rate K_{loc} is obtained using a stagnation-tangent method: a linear tangent is fitted using a fixed number of upstream samples adjacent to the $S_{u,ref}$ location (five points in the present work), and the negative slope of this tangent is taken as the local stretch rate, $K_{loc} = -dv/dy$. Each processed realisation therefore provides one ($S_{u,ref}$, K_{loc}) pair for the same operating condition.

For each fuel blend all the flame speed and local stretch rate pairs are plotted as a curve. However, as Wang et al. (2009) suggested, this requires the use of non-linear extrapolation curves to find laminar flame speed at zero stretch and so the curve from the corresponding simulation data is utilised to calculate the final values. The methodology for this combination continues in Section 2.3 following the methodology for the numerical work and largely follows methodology laid out by Zhang et al. (2014).

2.2 Simulation methodology

The simulations were all performed in ANSYS CHEMKIN using both the Opposed-flow Flame model in the Axisymmetric configuration and the Premixed Laminar Flame-Speed Calculation module. Mech_56.54 (Burke et al., 2015) was used for Fuels 1-3 and SanDiego (University of California at San Diego Chemical-Kinetic Mechanisms for Combustion Applications, 2023) was used for Fuels 4 and 5 due to the necessary extra include of butane chemistry for these fuel blends. Mech_56.54 was built upon NUIG Aramco1.3 (Metcalfe et al., 2013) but extended for use with DME and has been validated on a range of experimental methods including measurements of flame speeds (Burke et al., 2015). SanDiego is a reduced scope mechanism designed for use in flame conditions with more detailed species chains not included to reduce the computational cost of use.

A mechanism comparison was performed for Fuel 1 at stoichiometric conditions to identify the kinetic mechanism that best reproduces the measured stretch response. Figure 3 compares the experimentally derived $S_{u,ref}$ and K_{loc} data with simulations using Aramco 3.0 (Zhou et al., 2018), Mech_56.54, and SanDiego mechanisms. The Mech_56.54 predictions show the closest agreement with the experimental trend within the measured stretch range. This mechanism was therefore selected for subsequent simulations of Fuels 1 to 3.

The counterflow simulations were run using the Opposed-flow Flame model in the Axisymmetric configuration. The experimental conditions were represented in this model and details of the underpinnings of the model can be found in the CHEMKIN Theory Manual (ANSYS Inc, 2024). A mesh independence study was performed and it was found that a mesh of 800 was suitable for these simulations. Previous literature has also found meshes of similar densities yielded sufficient convergence for the Opposed-flow Flame model (Yang et al., 2021; Dames et al., 2016). Inlet velocities were varied from 0.5 m/s to 2.0 m/s in increments of 0.05 m/s while maintaining the same equivalence ratio, in order to generate a stretch rate range comparable to the experiments. Figure 4 shows representative centreline axial velocity profiles for Fuel 1 obtained using the Mech_56.54 mechanism. Taking the green line as an example, the vertical dashed line represents the flame front location for the condition with a 2 m/s inlet velocity. From this dashed line to the right the flow velocity can be seen to accelerate due to the thermal expansion effects and can then be seen to decrease in the post-flame region until the stagnation point. The particles then reverse direction due to the counterflow effect from the other modelled inlet. When adjusting the inlet velocity experimentally flow control valves were used to change the stretch condition while preserving the mixture composition and the simulated stagnation curves with varied inlet velocity provide the basis for extracting $S_{u,ref}$ and K_{loc} using the same analysis procedure applied to the experimental data.

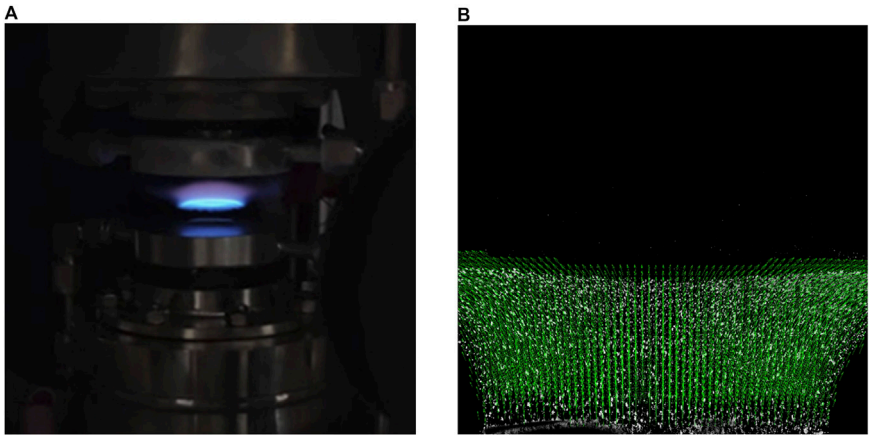

FIGURE 1
(A) Left; a true colour image of the flame sheet suspended between the two nozzles. **(B)** Right; the same flame processed using PIVlab. The points are the illuminated droplets of dimethyl silicone oil. The smear at the bottom left of the image is scattered light reflecting off the rear of the lower nozzle.

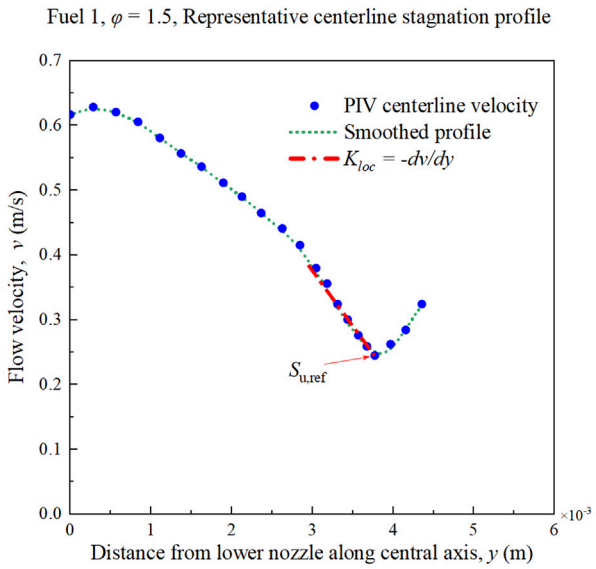

FIGURE 2
Representative centreline axial velocity profile v from time-resolved PIV for Fuel 1 at φ = 1.5 under a fixed condition. Blue markers are discrete PIV samples from image pairs, and the green dashed line is the smoothed profile used to determine. $S_{u,ref}$ as the upstream minimum of v and K_{loc} as the upstream maximum of $-dv/dy$.

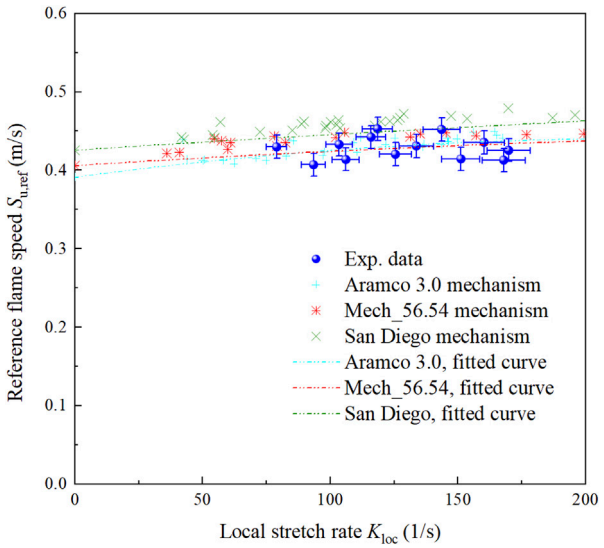

FIGURE 3
Reference flame speed $S_{u,ref}$ as a function of local stretch rate K_{loc} for Fuel 1 at φ = 1.0. Experimental data are compared with opposed flow simulations performed using three different kinetic mechanisms. Simulation results are shown as discrete point with fitted trends used to guide the comparison.

The axial velocity against distance curves were analysed using the stagnation tangent method described by Zhang (2017). The tangent is taken from a window corresponding to the same physical size with reference to the distance from nozzle axis as the one used in the lab experiment methodology from the curve before the minimum flame speed before the flame front. This tangent slope is the negative of the local stretch rate. These groups of flame speed and local stretch rate pairs can then be plotted for each fuel blend including the 1D laminar flame speed results to produce the curves used to compare against the experimental methodology.

2.3 Combined methodology

To construct the nonlinear extrapolation curves, a sixth-order polynomial representation was developed by combining freely propagating one-dimensional laminar flame calculations and opposed flow counterflow flame simulations. The 1D laminar flame calculations provide the unstretched laminar flame speed S_u^0 and are used to guide the intercept at $K_{loc} = 0$. The counterflow simulations provide the stretched response trend of $S_{u,ref}$ as a function of K_{loc}, with the simulated fields

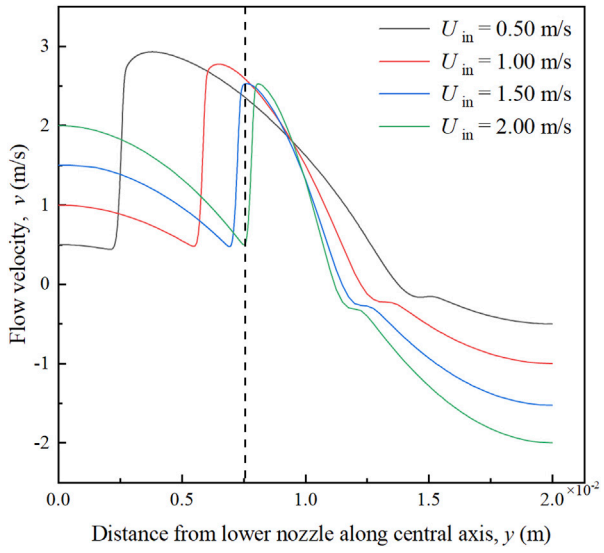

FIGURE 4
Representative centreline axial velocity profiles *v(y)* from opposed flow simulations for Fuel 1 at fixed φ using the Mech_56.54 mechanism. Each curve corresponds to a different inlet velocity, which produces a distinct stretch condition. The vertical dashed line represents the flame front location for the condition in green with a 2 m/s inlet velocity.

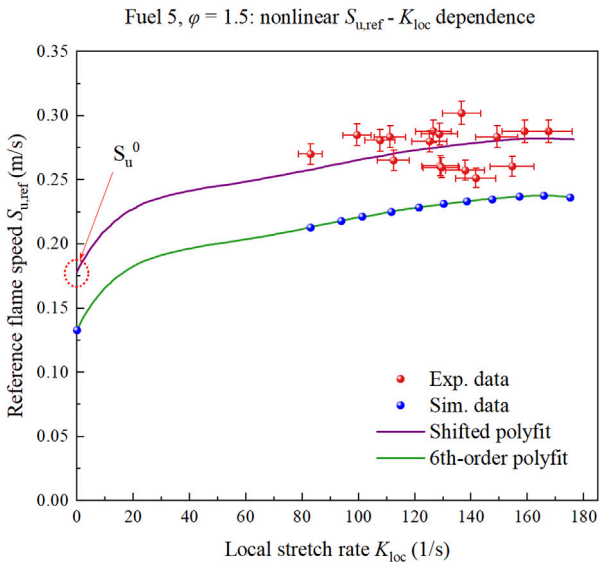

FIGURE 5
$S_{u,ref}$ as a function of K_{loc} for Fuel 5 at φ = 1.5. A sixth-order polynomial function is used to describe the nonlinear simulation trend, and the resulting curve is vertically shifted to pass through the experimental anchor point (guided by S_u^0) for extrapolation of the empirical laminar flame speed.

post processed in the same manner as the laboratory measurements.

The 1D flame speed simulations were performed using the Premixed Laminar Flame Speed Calculation module in ANSYS CHEMKIN. These simulations assume 1D flow with uniform inlet conditions and a premixed fuel air inflow. Automated grid refinement was used up to a prescribed maximum to support mesh optimisation. The simulations were conducted under adiabatic conditions at 15 °C and 1 atm, and further details of the model formulation are provided in the CHEMKIN PRO Theory Manual (ANSYS Inc, 2024).

The counterflow simulation results were analysed using the stagnation tangent methodology and associated uncertainty quantification described by Zhang (2017). The centreline axial velocity profile was evaluated within an upstream window that matches the physical size used in the experimental post processing. The reference flame speed $S_{u,ref}$ was identified from the minimum of the centreline velocity immediately upstream of the flame front. The local stretch rate K_{loc} was determined from the maximum magnitude of the centreline velocity gradient in the upstream evaluation region. The extracted [$S_{u,ref}$, K_{loc}] pairs were then obtained for each inlet velocity setting, which yields the simulated dependence of $S_{u,ref}$ on K_{loc} for each fuel blend at the prescribed equivalence ratio.

The extrapolation from stretched conditions to the unstretched laminar flame speed is nonlinear, therefore the polynomial curve must be adjusted to match the experimental data. A sixth-order polynomial was fitted to the simulation based $S_{u,ref}$ - K_{loc} relationship, with the intercept guided by the 1D value S_u^0. The resulting nonlinear curve was then vertically shifted using a least squares adjustment to best fit the experimental [$S_{u,ref}$, K_{loc}] data. The unstretched laminar flame speed S_u^0 was finally obtained from the intercept of the adjusted curve at K_{loc} = 0. An example of this procedure is shown in Figure 5, and the same approach was applied to all equivalence ratios and fuel blends.

3 Results

The methodology described above was applied to five LPG fuel blends over equivalence ratios from 0.75 to 1.6. The blend compositions were as specified in Table 1. In addition, measurements were performed for neat DME to enable comparison with prior literature that focuses on single component fuels.

Figure 6 presents the extracted unstretched laminar flame speed S_u^0 as a function of equivalence ratio for each fuel blend, together with the corresponding CHEMKIN predictions. For all blends, S_u^0 increases from the lean side and reaches a maximum close to stoichiometric conditions, followed by a decrease towards richer mixtures. Across the dataset, the peak typically occurs around φ between 1.0 and 1.1, with peak values in the range of approximately 0.40–0.45 m/s for the blends tested. This behaviour is consistent with the expected response of hydrocarbon based premixed flames, where the balance between reactant availability and thermal diffusivity yields an optimum near stoichiometric conditions.

Overall agreement between experimental results and simulations is satisfactory for most fuel blends and equivalence ratios. The dashed simulation curves capture both the location of the peak and the general curvature of the S_u^0 trends. The most noticeable mismatch occurs for Fuel 1 under rich conditions, particularly for φ between 1.1 and 1.5, where the simulations predict higher flame speeds than those inferred from the experiment. Several factors may contribute to this discrepancy. First, the rich side measurements are more sensitive to the stretch correction and to the extrapolation procedure because the curvature of the $S_{u,ref}$ versus K_{loc} relation becomes more pronounced,

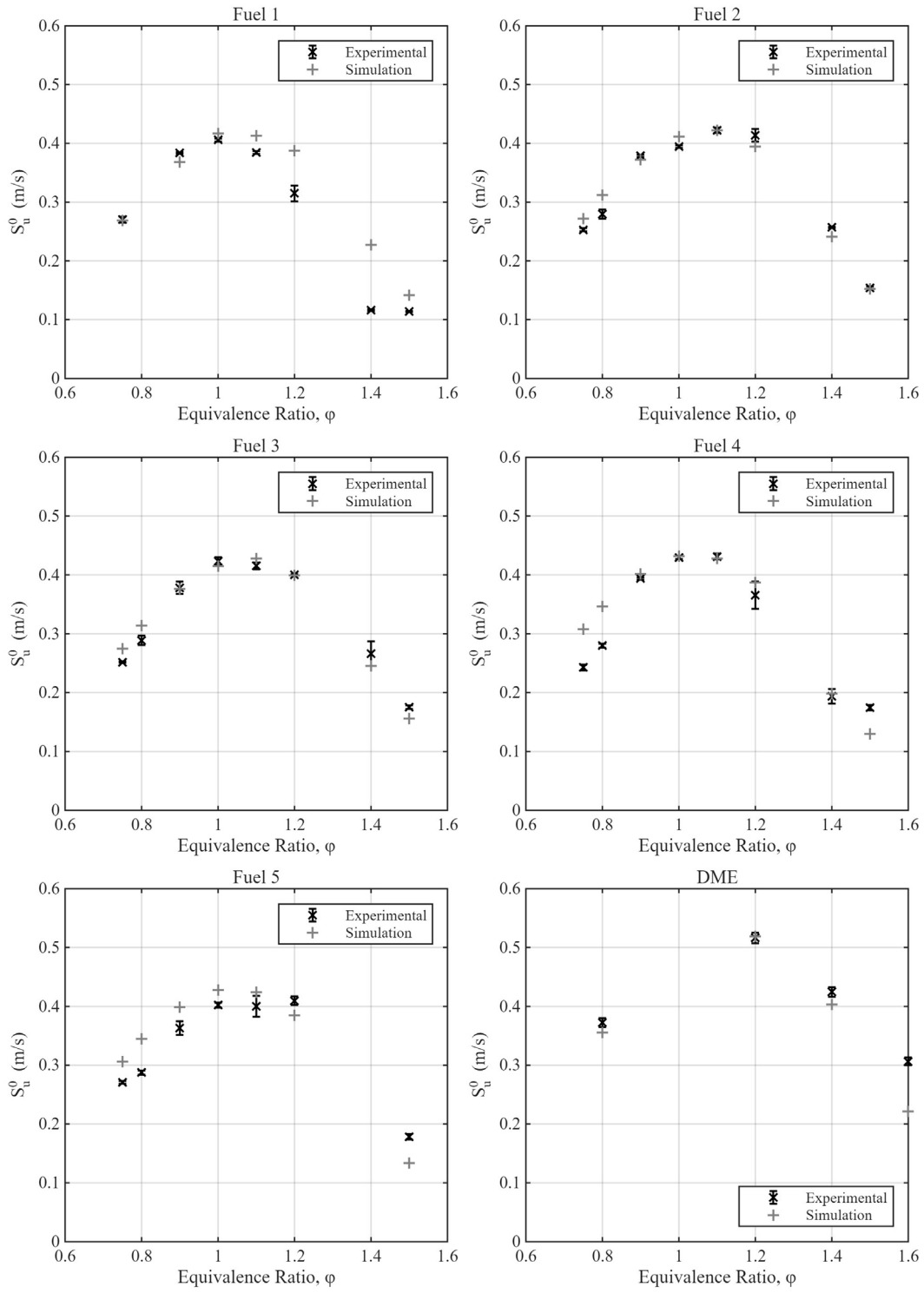

FIGURE 6
A comparison of Flame Speed against Equivalence Ratio plots for all of the fuels tested comparing the final results with shaded error margins against the simulated curves produced using Ansys CHEMKIN.

which increases the influence of uncertainty in K_{loc} extraction. Second, the chemical mechanism may have larger uncertainty in rich chemistry pathways for the specific blend composition. These explanations are consistent with the observation that the deviation is most evident in the fuel blend with the highest propane fraction.

Figure 7 overlays the experimentally determined S_u^0 values for all fuels, allowing a direct comparison of composition effects across equivalence ratio. Overall, the results all show the data trend expected from their constituent fuels however there are some differences from what would be expected. The fuel blends display much narrower

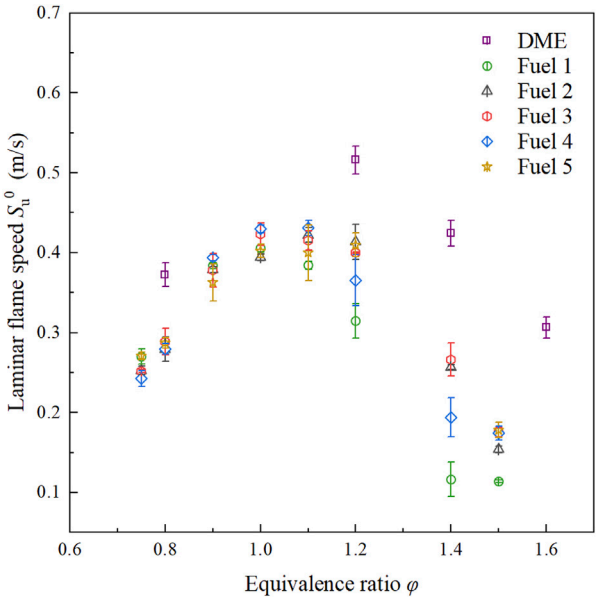

FIGURE 7
Overlaid flame speed data for the five fuel blends tested and DME.

variation on the leaner side of combustion including stochiometric conditions which should ease the introduction of new standards as the majority of home appliances are designed to run in these conditions. Fuel 1 with the highest propane fraction predictably drops down lower in leaner conditions. The flat tail of the curve is believed to not be how the fuel would behave if tested over a large enough data set and was similarly seen in Fuel 4. However, Fuel 1 could be caused by lower numbers of valid results causing it to be less simulation independent for 1.5 compared to 1.2 and 1.4. Fuel 4 could be showing the same behaviour but instead showing it for 1.4 thereby causing 1.5 to look overly skewed away from the simulations. Fuel 3 whilst not showing the highest flame speed on the lowest equivalence ratio does display the highest flame speed for the rest of the curve due the addition of the propylene as well as the 20% DME fraction contained in Fuel 2 to Fuel 5. Since the current specification for propane can include a fraction of propylene this would need to be taken into account as it raises the risk of the addition of DME raising the flame speed out of specification.

The uncertainty bars shown in Figure 6 and the scatter in Figure 7 indicate that the largest experimental uncertainty occurs around φ equal to 1.1 and 1.2. This behaviour is consistent across multiple fuels. A plausible explanation is that flame luminosity increases around these equivalence ratios, leading to elevated background intensity in the recorded images. Increased background intensity can degrade the quality of the PIV correlation peak detection and reduce the robustness of the post processing used to extract the stagnation profile, which propagates into uncertainty in both $S_{u,ref}$ and K_{loc}, and ultimately into the extrapolated S_u^0. This effect is particularly evident for Fuel 4, which shows stronger luminous interference and correspondingly larger uncertainty. These observations support the need to treat optical background management and image quality control as key contributors to the uncertainty budget for PIV based counterflow flame speed measurements.

While Figures 6, 7 present fuel specific flame speed trends as a function of equivalence ratio, two additional analyses were performed to strengthen the interpretation of the results. Figure 8 benchmarks the present measurements and simulations against literature laminar flame speed datasets for the main neat fuel components, providing an external consistency check at comparable ambient conditions. Figure 9 then summarizes the overall agreement between simulations and the experimentally inferred S_u^0 values using a parity plot, which enables a compact assessment of systematic bias across all fuels.

Figure 8 shows a range of literature laminar flame speeds for DME, propylene, propane, n-butane, and i-butane at near ambient conditions that are comparable to the present experiments. The CHEMKIN simulations produced in this work fall within the literature envelopes for the five neat fuels over the equivalence ratio range relevant to the LPG blend measurements. This comparison supports the use of the selected kinetic mechanisms as a physically consistent basis for the simulation guided nonlinear extrapolation applied to the blend data.

Figure 9 compares the experimental S_u^0 results produced in this paper to S_u^0 of fuel blends calculated through interpolation of simulated S_u^0 of pure fuels. Most points lie within the ±20% envelope, indicating that agreement is not confined to a single fuel or a narrow equivalence ratio band. This comparison is not an intended to be an analysis of the mechanisms used to simulate the flame speeds of the pure fuels but instead to compared the differences between S_u^0 of fuel blends when measured accurately compared to using a substitute method of calculation. This interpolation method has been known to be used in industry and as shown the majority of points lie within the 20% discrepancy margin and the trendlines are all within 8% discrepancy.

4 Conclusion

Unstretched laminar flame speeds were measured for five DME blended LPG mixtures and pure DME over equivalence ratios from 0.75 to 1.6 using a counterflow premixed configuration with PIV based stagnation analysis. The reference flame speed and local stretch rate were extracted from the centreline velocity minimum upstream of the flame front and the maximum upstream velocity gradient, and S_u^0 was obtained using a simulation guided nonlinear extrapolation anchored by one dimensional freely propagating flame calculations.

All blends show a peak in S_u^0 near stoichiometric conditions, with blend peak values around 0.40–0.45 m/s. Inter blend variation is limited on the lean side and increases under rich conditions, and the propylene containing blend exhibits elevated flame speeds across much of the range. The largest uncertainty occurs around φ = 1.1 to φ = 1.2, consistent with increased luminosity and reduced robustness of PIV based gradient extraction.

CHEMKIN captures the main S_u^0 trends, with Mech_56.54 selected for Fuels 1 to 3 and the San Diego mechanism used for butane containing blends. A parity assessment shows most results within ±20%, with modest over prediction for blends and under prediction for neat DME. Future work should repeat the measurements using pulsed laser illumination and appropriate optical filtering to suppress flame luminosity and improve image contrast, which is expected to reduce the

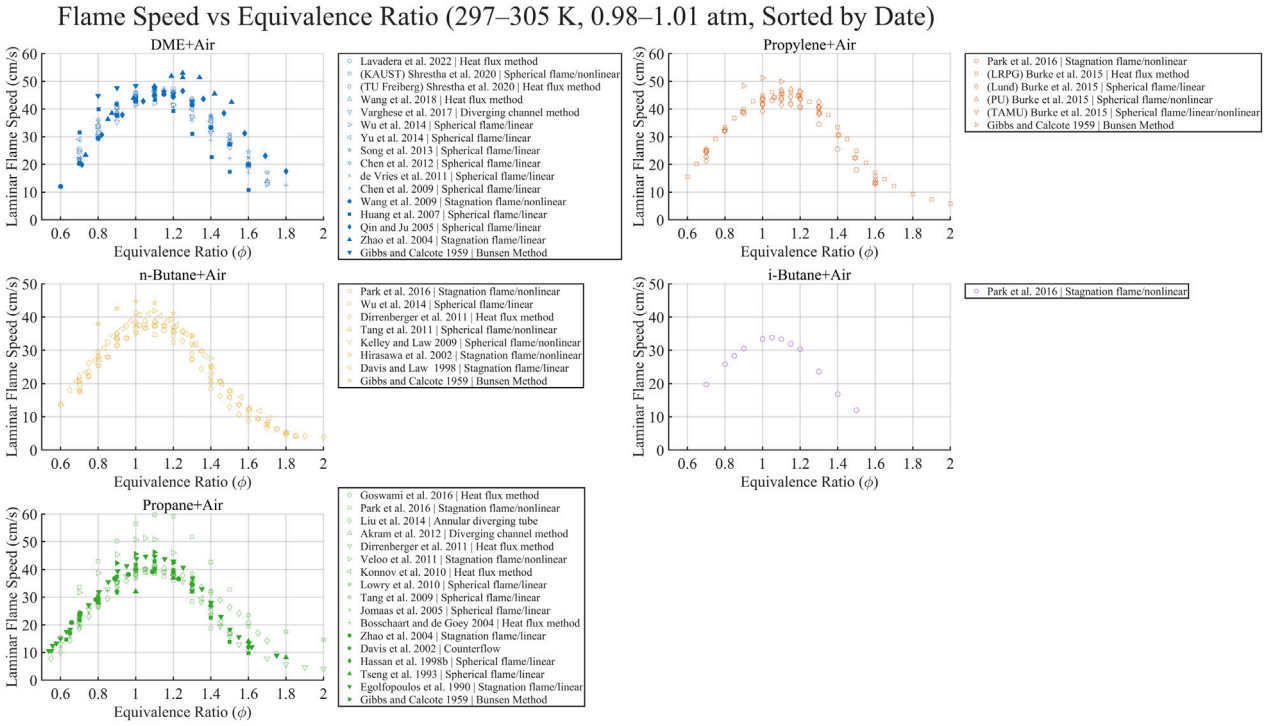

FIGURE 8
Literature laminar flame speeds for DME, propylene, propane, n-butane, and i-butane at near ambient conditions.

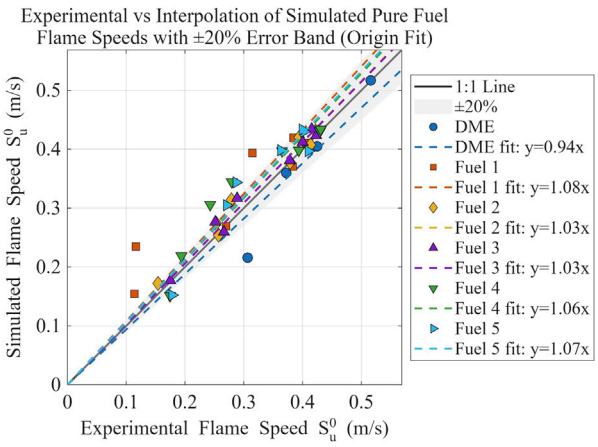

FIGURE 9
Parity plot of S_u^0 of fuel blends calculated through interpolation of simulated S_u^0 of pure fuels versus experimental S_u^0 for all fuels, with a ±20% envelope and fuel specific trendlines.

uncertainty in the extracted velocity gradients and therefore tighten the reported error margins.

The dataset will be useful for the production of chemical kinetics mechanism which will assist in the adoption of lower carbon fuels. These data can also be used as a reference point for the production of industrial standards and by increasing the datasets available for public reference a more accurate understanding of flame speed and the overall behaviour of hydrocarbon and DME blends can be gained.

Data availability statement

The original contributions presented in the study are included in the article/supplementary material, further inquiries can be directed to the corresponding author.

Author contributions

JW: Conceptualization, Formal Analysis, Investigation, Methodology, Resources, Validation, Visualization, Writing – original draft, and Writing – review and editing. DL: Writing – review and editing, Writing – original draft. YC: Writing – review and editing, Writing – original draft. YZ: Methodology, Resources, Writing – review and editing. RY: Conceptualization, Resources, Writing – review and editing.

Funding

The author(s) declared that financial support was received for this work and/or its publication. The authors would like to acknowledge CASE studentship, the International Student Visiting Scholar Funding Program of Tsinghua University, and EPSRC for the funding support of the research project (Grant Ref: EP/W524360/1, EP/Y020839/1). For the purpose of open access, the author has applied a 'Creative Commons Attribution (CC BY) licence to any Author Accepted Manuscript version arising.

Conflict of interest

The author(s) declared that this work was conducted in the absence of any commercial or financial relationships that could be construed as a potential conflict of interest.

The author RY declared that they were an editorial board member of Frontiers at the time of submission. This had no impact on the peer review process and the final decision.

Generative AI statement

The author(s) declared that generative AI was not used in the creation of this manuscript.

Any alternative text (alt text) provided alongside figures in this article has been generated by Frontiers with the support of artificial intelligence and reasonable efforts have been made to ensure accuracy, including review by the authors wherever possible. If you identify any issues, please contact us.

Publisher's note

All claims expressed in this article are solely those of the authors and do not necessarily represent those of their affiliated organizations, or those of the publisher, the editors and the reviewers. Any product that may be evaluated in this article, or claim that may be made by its manufacturer, is not guaranteed or endorsed by the publisher.

References

ANSYS Inc (2024). *Ansys® Chemkin Theory Manual.*

Burke, U., Somers, K. P., O'Toole, P., Zinner, C. M., Marquet, N., Bourque, G., et al. (2015). An ignition delay and kinetic modeling study of methane, dimethyl ether, and their mixtures at high pressures. *Combust. Flame* 162 (2), 315–330. doi:10.1016/j.combustflame.2014.08.014

Chen, Z. (2015). On the accuracy of laminar flame speeds measured from outwardly propagating spherical flames: methane/air at normal temperature and pressure. *Combust. Flame* 162 (6), 2442–2453. doi:10.1016/j.combustflame.2015.02.012

Cheng, Z., Pitz, R. W., and Wehrmeyer, J. A. (2006). Lean and ultralean stretched propane–air counterflow flames. *Combust. Flame* 145 (4), 647–662. doi:10.1016/j.combustflame.2006.02.006

Daly, C. A., Simmie, J. M., Würmel, J., DjebaÏli, N., and Paillard, C. (2001). Burning velocities of dimethyl ether and air. *Combust. Flame* 125 (4), 1329–1340. doi:10.1016/S0010-2180(01)00249-8

Dames, E. E., Rosen, A. S., Weber, B. W., Gao, C. W., Sung, C.-J., and Green, W. H. (2016). A detailed combined experimental and theoretical study on dimethyl ether/propane blended oxidation. *Combust. Flame* 168, 310–330. doi:10.1016/j.combustflame.2016.02.021

Davis, S. G., and Law, C. K. (1998). Determination of and fuel structure effects on laminar flame speeds of C1 to C8 hydrocarbons. *Combust. Sci. Technol.* 140 (1-6), 427–449. doi:10.1080/00102209808915781

de Vries, J., Lowry, W. B., Serinyel, Z., Curran, H. J., and Petersen, E. L. (2011). Laminar flame speed measurements of dimethyl ether in air at pressures up to 10atm. *Fuel* 90 (1), 331–338. doi:10.1016/j.fuel.2010.07.040

Egolfopoulos, F. N., Hansen, N., Ju, Y., Kohse-Höinghaus, K., Law, C. K., and Qi, F. (2014). Advances and challenges in laminar flame experiments and implications for combustion chemistry. *Prog. Energy Combust. Sci.* 43, 36–67. doi:10.1016/j.pecs.2014.04.004

Jayachandran, J., Lefebvre, A., Zhao, R., Halter, F., Varea, E., Renou, B., et al. (2015). A study of propagation of spherically expanding and counterflow laminar flames using direct measurements and numerical simulations. *Proc. Combust. Inst.* 35, 695–702. doi:10.1016/j.proci.2014.05.031

Konnov, A. A., Mohammad, A., Kishore, V. R., Kim, N. I., Prathap, C., and Kumar, S. (2018). A comprehensive review of measurements and data analysis of laminar burning velocities for various fuel+air mixtures. *Prog. Energy Combust. Sci.* 68, 197–267. doi:10.1016/j.pecs.2018.05.003

Lewis, B., and Von Elbe, G. (1934). Determination of the speed of flames and the temperature distribution in a spherical bomb from time-pressure explosion records. *J. Chem. Phys.* 2 (5), 283–290. doi:10.1063/1.1749464

Metcalfe, W. K., Burke, S. M., Ahmed, S. S., and Curran, H. J. (2013). A hierarchical and comparative kinetic modeling study of C1 – C2 hydrocarbon and oxygenated fuels. *Int. J. Chem. Kinet.* 45 (10), 638–675. doi:10.1002/kin.20802

Movaghar, A., Lawson, R., and Egolfopoulos, F. N. (2020). Confined spherically expanding flame method for measuring laminar flame speeds: revisiting the assumptions and application to C1C4 hydrocarbon flames. *Combust. Flame* 212, 79–92. doi:10.1016/j.combustflame.2019.10.023

Qin, X., and Ju, Y. (2005). Measurements of burning velocities of dimethyl ether and air premixed flames at elevated pressures. *Proc. Combust. Inst.* 30 (1), 233–240. doi:10.1016/j.proci.2004.08.251

Safdari, A., Yovino, L., Kim, G., Rahman, R. K., and Vasu, S. S. (2025). "Laminar burning speed measurements of DME-hydrocarbon mixtures," in *ASME Turbo Expo 2025: Turbomachinery Technical Conference and Exposition*.

Song, W. S., Jung, S. W., Park, J., Kwon, O. B., Kim, Y. J., Kim, T. H., et al. (2013). Effects of syngas addition on flame propagation and stability in outwardly propagating spherical dimethyl ether-air premixed flames. *Int. J. Hydrogen Energy* 38 (32), 14102–14114. doi:10.1016/j.ijhydene.2013.08.037

Thielicke, W. (2014). *The Flapping Flight of Birds: Analysis and Application. Doctor of Philosophy Thesis Fully Internal (DIV).* University of Groningen. e30.

Thielicke, W. (2022). Pulse-length induced motion blur in PIV particle images: to be avoided at any cost? *Proc. Fachtagung Exp. Strömungsmechanik* 6 (8) 4.1–4.8.

Thielicke, W., and Sonntag, R. (2021). Particle image velocimetry for MATLAB: Accuracy and enhanced algorithms in PIVlab. *J. Open Res. Softw.* 9, 12. doi:10.5334/jors.334

Thielicke, W., and Stamhuis, E. J. (2014). PIVlab – towards user-friendly, affordable and accurate digital particle image velocimetry in MATLAB. *J. Open Res. Softw.* 2. doi:10.5334/jors.bl

University of California at San Diego Chemical-Kinetic Mechanisms for Combustion Applications (2023). *San Diego Mechanism Web Page: Mechanical and Aerospace Engineering (Combustion Research)*. Available online at: http://combustion.ucsd.edu (Accessed June 23, 2023).

Wang, Y. L., Holley, A. T., Ji, C., Egolfopoulos, F. N., Tsotsis, T. T., and Curran, H. J. (2009). Propagation and extinction of premixed dimethyl-ether/air flames. *Proc. Combust. Inst.* 32 (1), 1035–1042. doi:10.1016/j.proci.2008.06.054

Wu, H., Hu, E., Yu, H., Li, Q., Zhang, Z., Chen, Y., et al. (2014). Experimental and numerical study on the laminar flame speed of n-Butane/Dimethyl ether–air mixtures. *Energy & Fuels* 28 (5), 3412–3419. doi:10.1021/ef402502w

Xiouris, C., Ye, T., Jayachandran, J., and Egolfopoulos, F. N. (2016). Laminar flame speeds under engine-relevant conditions: uncertainty quantification and minimization in spherically expanding flame experiments. *Combust. Flame* 163, 270–283. doi:10.1016/j.combustflame.2015.10.003

Yang, X., Wu, Y., Zhang, Y., Zhang, H., and Zhang, J. (2021). Reassessing the 2-D velocity boundary effect on the determination of extinction stretch rate and laminar flame speed using the counterflow flame configuration. *Combust. Flame* 234, 111630. doi:10.1016/j.combustflame.2021.111630

Yu, H., Hu, E., Cheng, Y., Zhang, X., and Huang, Z. (2014). Experimental and numerical study of laminar premixed dimethyl ether/methane–air flame. *Fuel* 136, 37–45. doi:10.1016/j.fuel.2014.07.032

Zhang, Y. (2017). *Propagation and Extinction Studies of Laminar Lean Premixed Syngas/Air Flames.* Springer.

Zhang, Y., Shen, W., Fan, M., Zhang, H., and Li, S. (2014). Laminar flame speed studies of lean premixed H2/CO/air flames. *Combust. Flame* 161 (10), 2492–2495. doi:10.1016/j.combustflame.2014.03.016

Zhou, C.-W., Li, Y., Burke, U., Banyon, C., Somers, K. P., Ding, S., et al. (2018). An experimental and chemical kinetic modeling study of 1,3-butadiene combustion: ignition delay time and laminar flame speed measurements. *Combust. Flame* 197, 423–438. doi:10.1016/j.combustflame.2018.08.006